JACC: CLINICAL ELECTROPHYSIOLOGY VOL. 7, NO. 6, 2021

NEW RESEARCH PAPERS

BASIC AND TRANSLATIONAL SCIENCE

Endo-Epicardial Mapping of In Vivo Human Sinoatrial Node Activity

Rohit K. Kharbanda, MD,[a,b,*] Fons J. Wesselius, MSc,[a,*] Mathijs S. van Schie, MSc,[a] Yannick J.H.J. Taverne, MD, PhD,[b] Ad J.J.C. Bogers, MD, PhD,[b] Natasja M.S. de Groot, MD, PhD[a]

ABSTRACT

OBJECTIVES The aim of the current study was to examine electrophysiological characteristics of sinoatrial node (SAN) activity from an endo-epicardial perspective.

BACKGROUND Electrophysiological properties of the in vivo human SAN and its exit pathways remain poorly understood.

METHODS Twenty patients (75% male; median age 66 years [59 to 73 years]) with structural heart disease underwent simultaneous endo-epicardial mapping (256 unipolar electrodes, interelectrode distance 2 mm). Conduction times, endo-epicardial delays (EEDs), and R/S ratio were examined in the surrounding 10 mm of SAN activation. Areas of conduction block were defined as conduction delays ≥12 ms and endo-epicardial asynchrony as EED ≥15 m.

RESULTS Three distinct activation patterns were observed in a total of 28 SAN-focal activation patterns (SAN-FAPs) (4 patients exhibited >1 different exit site), including SAN activation patterns with: 1) solely an endocardial exit site (n = 10 [36%]); 2) solely an epicardial exit site (n = 13 [46%]); and 3) simultaneously activated endo-epicardial exit sites (n = 5 [18%]). Median (interquartile range) EED at the origin of the SAN-FAP was 10 ms (6 to 14 ms) and the prevalence of endo-epicardial asynchrony in the surroundings of the SAN-FAP was 5% (2% to 18%). Electrograms at the origin of the SAN-FAPs exhibited significantly larger R-peaks in the mid right atrium (RA) compared with the superior RA (mid R/S ratio 0.15 [0.067 to 0.34] vs. superior R/S ratio 0.045 [0.026 to 0.062]; p = 0.004). Conduction velocity within a distance of 10 mm from the SAN-FAP was 125 cm/s (80 to 250 cm/s). All 6 SAN-FAPs at the mid RA were observed in patients with a history of atrial fibrillation.

CONCLUSIONS Variations in activation patterns of the SAN observed in this study highlight the complex 3-dimensional SAN geometry and indicate the presence of interindividual differences in SAN exit pathways. Solely in patients with a history of atrial fibrillation, SAN activity occurred more caudally, which indicates changes in preferential SAN exit pathways. (J Am Coll Cardiol EP 2021;7:693–702) © 2021 The Authors. Published by Elsevier on behalf of the American College of Cardiology Foundation. This is an open access article under the CC BY-NC-ND license (http://creativecommons.org/licenses/by-nc-nd/4.0/).

From the [a]Department of Cardiology, Erasmus Medical Center, Rotterdam, the Netherlands; and the [b]Department of Cardio-thoracic Surgery, Erasmus Medical Center, Rotterdam, the Netherlands. *Dr. Kharbanda and Mr. Wesselius contributed equally to this work.

The authors attest they are in compliance with human studies committees and animal welfare regulations of the authors' institutions and Food and Drug Administration guidelines, including patient consent where appropriate. For more information, visit the Author Center.

Manuscript received July 21, 2020; revised manuscript received October 8, 2020, accepted November 18, 2020.

ISSN 2405-500X https://doi.org/10.1016/j.jacep.2020.11.017

ABBREVIATIONS AND ACRONYMS

AF = atrial fibrillation
AFL = atrial flutter
CB = conduction block
CV = conduction velocity
EEA = endo-epicardial asynchrony
EED = endo-epicardial delay
LAT = local activation time
LVF = left ventricular function
RA = right atrium
SAN = sinoatrial node
SAN-FAP = sinoatrial focal activation pattern
SR = sinus rhythm

Propagation of the electrical wave front from the sinoatrial node (SAN) into the surrounding atrial tissue is a complex 3-dimensional process. Boineau et al. (1) and Schuessler (2) postulated that the SAN is isolated from the right atrial myocardium by the SAN artery and fibro-fatty tissue except for several exit pathways. These exit pathways enable atrial excitation at multiple sites simultaneously and are influenced by neurohormonal factors. Subsequently, Fedorov et al. (3) used optical mapping of the isolated coronary-perfused human SAN in combination with histological examination to show that SAN arteries and fibrotic and fatty tissue surrounding the SAN indeed form significant conduction barriers. By showing that propagation from the SAN occurred via multiple sinoatrial exit pathways bypassing these structural barriers, the Boineau and Schuessler hypothesis was further substantiated. A recent study by Bychkov et al. (4) in ex vivo mice provided novel insights into the role of subcellular Ca^{2+} signaling pathways within and among cells comprising the SAN. Microscopic assessment of the SAN revealed synchronized action potentials emerging from heterogeneous subcellular subthreshold Ca^{2+} currents, which highlight the functional complexity of the SAN. Although the SAN was described more than a century ago, the electrophysiological properties of the SAN and its sinoatrial exit pathways remain poorly understood.

Sánchez-Quintana et al. (5) studied the architecture of the SAN in 47 postmortem hearts. They found that the SAN is a highly complex irregular structure packed within a dense matrix of connective tissue with multiple radiations interdigitating with the surrounding myocardium. The authors postulated that the anatomy of the SAN may facilitate slowing of conduction, thereby providing a substrate for reentry. Recent data suggest that SAN activity provokes endocardial-epicardial asynchrony (EEA) (6). Whether structural barriers surrounding the SAN also result in enhanced conduction abnormalities between the endocardial and/or epicardial layer is unknown.

SEE PAGE 703

Thus far, few studies have described the simultaneously occurring patterns of activation in the endo- and epicardial layer surrounding the SAN area in the intact human heart. We therefore investigated SAN activation in patients undergoing open heart surgery by performing simultaneous endo-epicardial mapping at a high-density scale.

METHODS

STUDY POPULATION. Patients with structural heart disease undergoing elective open heart surgery were

FIGURE 1 Simultaneous Endo-Epicardial Mapping of the Right Atrium

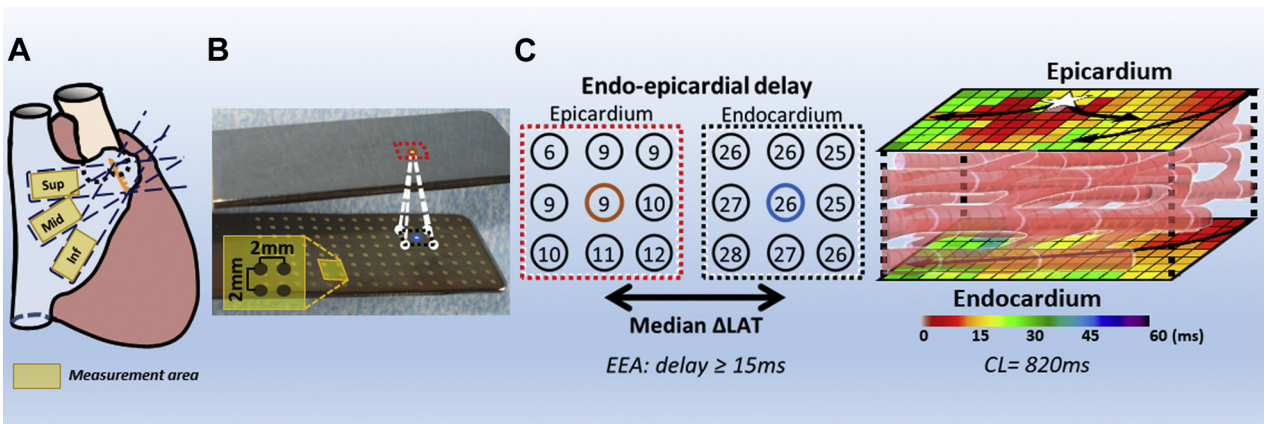

(A) Two 128-electrode arrays were secured exactly opposite of each other on 2 spatulas (Ø electrode = 0.45 mm, interelectrode distance = 2 mm). One spatula was placed in the right atrium on the endocardial surface through the incision for venous cannulation. The other spatula was placed on the opposite epicardial surface. Recordings were performed at 3 locations, toward the superior cava vein (superior [Sup]), the terminal crest (Mid), and the inferior cava vein (inferior [Inf]). **(B)** To calculate endocardial-epicardial delay (EED), the local activation times of the direct opposite electrode and its 8 surrounding electrodes were used. **(C)** Color-coded activation map of the endocardium and epicardium covering the sinoatrial node region demonstrating an epicardial sinoatrial node exit site. EED was calculated by determining local endo-epicardial activation time differences. For each electrode, the median of the time delays within the exact opposite electrode and its 8 surrounding electrodes was selected. Endo-epicardial asynchrony (EEA) was defined as EED ≥15 ms. CL = cycle length; LAT = local activation time.

TABLE 1 Patient Characteristics

Number of patients with SAN-FAPs	20
Age (yrs)	66 (59-73)
Male	15 (75.0)
BMI (kg/m^2)	27 (23-31)
Underlying heart disease	
iHD	9 (45.0)
vHD	4 (20.0)
cHD	7 (35.0)
History of AF	
Paroxysmal AF	8 (40.0)
Cardiovascular risk factors	
Hypertension	10 (50.0)
Diabetes mellitus	7 (35.0)
Hypercholesterolemia	10 (50.0)
LVF	
Good or mild impairment (LVEF ≥40%)	17 (85.0)
Moderate impairment (LVEF 30%–39%)	3 (15.0)

Values are n, median (interquartile range), or n (%).

AF = atrial fibrillation; BMI = body mass index; cHD= combined heart disease; iHD = ischemic heart disease; LVF = left ventricular function; LVEF = left ventricular ejection fraction; SAN-FAPs = sinoatrial node-focal activation patterns; vHD= valvular heart disease.

included in the current study. Exclusion criteria were hemodynamic instability, implanted pacemaker with atrial pacing, previous cardiac surgery, end-stage renal failure, or severely impaired left ventricular function. The study was approved by the institutional medical ethical committee (MEC2015-373), and written informed consent was obtained from all patients. The study was performed according to the principles of the Declaration of Helsinki. Patient characteristics were obtained from electronic medical files.

SIMULTANEOUS ENDO-EPICARDIAL MAPPING PROCEDURE. An overview of the methodology is provided in Figure 1. After heparinization and arterial cannulation, simultaneously endo- and epicardial mapping was performed before commencement of extracorporeal circulation. Two electrode arrays, each containing 128 unipolar electrodes with a diameter of 0.45 mm and 2 mm interelectrode spacing, were secured on 2 bendable spatulas. As shown in Figure 1B, the electrode arrays were located on the exact opposite side of each other (7). A temporary epicardial pacemaker wire was stitched to the RA free wall and served as the reference electrode. The indifferent electrode was connected to a steel wire, which was stitched to the subcutaneous tissue of the thoracic wall. Before venous cannulation, one spatula (marked as the endocardial electrode array) was introduced in the right atrium (RA) after incising the right atrial appendage, and the incision site was closed with the purse string suture. To prevent overlap of measurement area near the right atrial incision, the endocardial electrode array was introduced into the RA for at least 1.5 cm extra after introducing the last row of electrodes.

TABLE 2 Characteristics of SAN-FAPs

Number of SAN-FAPs	28
Repetitive	25 (89.0)
Near lines of CB	16 (57.0)
RA location	
Superior	22 (79.0)
Middle	6 (21.0)
Inferior	0 (0.0)
Layer of exit site	
Epicardial exit site	13 (46.0)
Endocardial exit site	10 (36.0)
Endo- and epicardial exit sites	5 (18.0)
CL (ms)	
Median	793 (672–964)
Superior	829 (705–938)
Mid	545 (417–1,009)

Values are n, n (%), or median (interquartile range).

CB = conduction block; CL = cycle length; RA = right atrial; other abbreviations as in Table 1.

Simultaneous endo-epicardial mapping was performed following a predefined mapping scheme with 3 different mapping locations on the right atrial free wall as illustrated in Figure 1A. Mapping of the superior RA started at the junction of the superior cava vein and RA also covering the sulcus terminalis. Due to the large dynamic range of SAN activity, the mapping clamp was subsequently moved to the middle and inferior part of the RA.

Simultaneous endo-epicardial mapping was performed for 5 s during sinus rhythm (SR) and included a calibration signal of 2 mV and 1,000 ms, a bipolar reference electrogram, and all endo- and epicardial unipolar electrograms. Recordings were analogue-to-digital converted (16-bits), sampled with a rate of 1 kHz, amplified (gain 1,000), and filtered (bandwidth 0.5 to 400 Hz).

MAPPING DATA ANALYSIS. Mapping data were analyzed by using custom-made software previously described in detail (8). For both the endo- and epicardial layer, color-coded activation maps were reconstructed by annotating the steepest negative slope of atrial potentials recorded at every electrode (9). Consistent with previous intraoperative mapping studies, areas of conduction block (CB) were defined as interelectrode differences in local activation times (LATs) ≥12 ms corresponding with effective conduction velocities <17 cm/s.

SAN ACTIVATION. All recordings were independently screened by 2 researchers based on the selection criteria for FAPs, as described in previous studies (9–11). These criteria include: 1) the electrode from

FIGURE 2 **3-Dimensional Dynamics of Sinoatrial Node Activation**

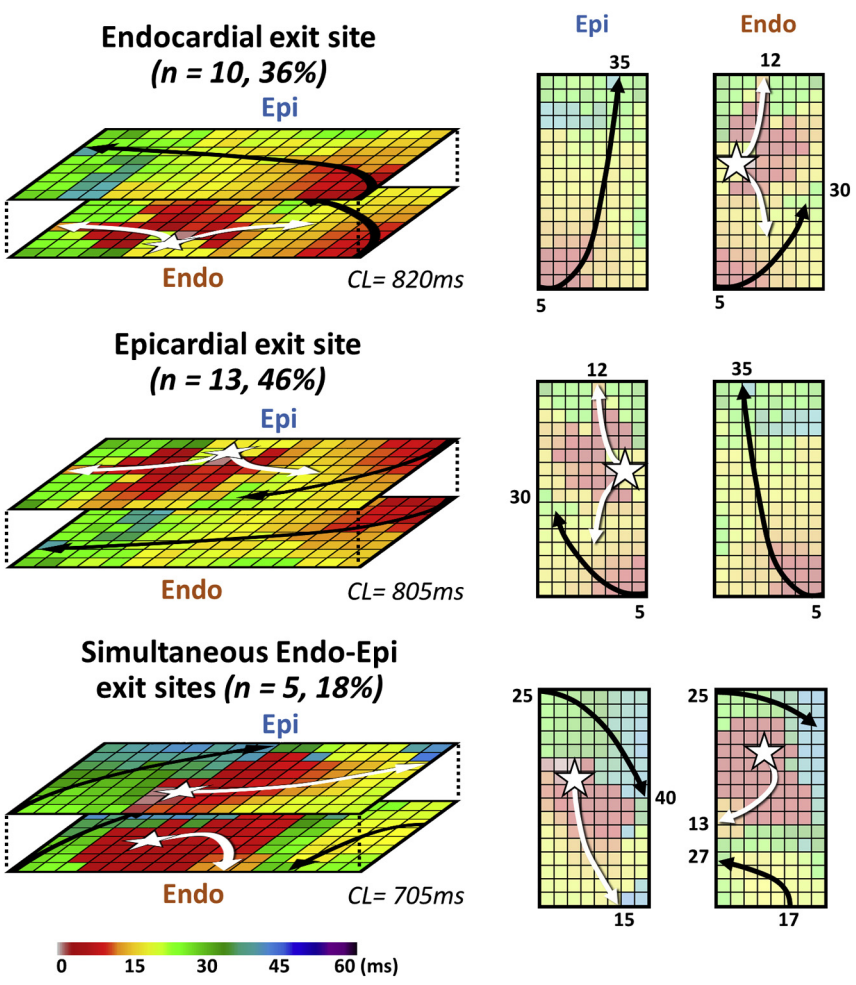

Three types of sinoatrial node–focal activation patterns (SAN-FAPs) were observed: 1) solely an endocardial exit site (**upper panel**; n = 10 [36%]); 2) solely an epicardial exit site (**middle panel**; n = 13 [46%]; and 3) simultaneously activated endo-epicardial exit sites (**lower panel**; n = 5 [18%]). **Stars** indicate origins of SAN-FAPs, and **arrows** indicate the main trajectories of the SAN-FAP. Local activation times are depicted near the head and tail of the **arrows**. CL = cycle length; Endo = endocardium; Epi = epicardium.

which the SAN-FAP originates (SAN-FAP origin) is not activated >1 ms after activation of the first electrode of the entire electrode array; 2) in case of a neighboring electrode being activated at the same time, this electrode should be activated at least 2 ms earlier than its surrounding electrodes; and 3) the distance between the border of the mapping area and the SAN-FAP origin should be at least 2 electrodes.

In case of repetitive SAN activation patterns that were nearly distinguishable from one another, only one SAN-FAP arising at the same location during the entire recording was included for analyses. If the SAN-FAP origin covered more electrodes with similar LATs, the electrode closest to the center of this earliest activated area was chosen as the SAN-FAP origin. To investigate conduction properties at different distances relative to the SAN-FAP origin, the Euclidean distances between the SAN-FAP origin and surrounding electrodes within a range of 10 mm were calculated. This yielded 14 predefined distances from the SAN-FAP origin: 0 mm (origin), 2, 2.8, 4.0, 4.5, 5.6, 6.0, 6.3, 7.2, 8.0, 8.2, 8.5, 8.9, and 10.0 mm. SAN-FAPs with their origin within a range of 6 mm from a line of CB were labeled as FAPs near lines of CB.

FIGURE 3 Spatial Distribution and Electrogram Fingerprint of Sinoatrial Node Activation

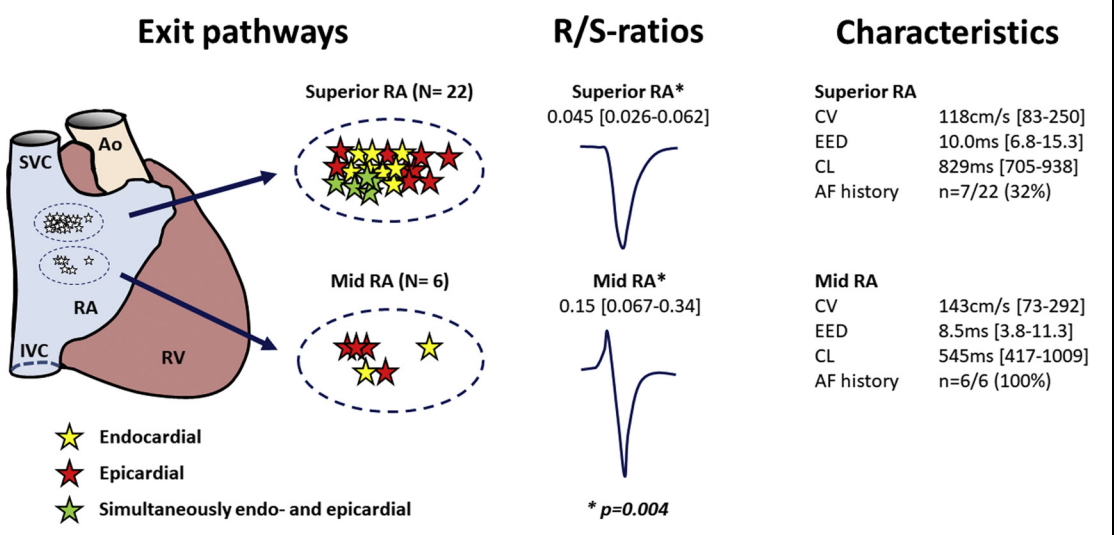

(Left) Distribution of SAN-FAP exit pathways are illustrated per location and per layer separately. **Yellow, red, and green stars** indicate SAN-FAPs with endocardial-, epicardial-, and simultaneous endo-epicardial exit sites, respectively. **(Middle)** R/S ratio at the origin of SAN-FAPs specified per location. A significant difference in the R/S ratio was observed between the superior right atrium (RA) and mid RA ($p = 0.004$). **(Right)** Characteristics of SAN-FAPs in the superior RA and mid RA. AF = atrial fibrillation; Ao = aorta; CV = conduction velocity; IVC = inferior vena cava; RV = right ventricle; SVC = superior vena cava; other abbreviations as in Figures 1 and 2.

PROPAGATION OF SAN-FAPs IN EITHER THE ENDOCARDIUM OR EPICARDIUM. Conduction velocity (CV) in an area with a radius of 10 mm around the SAN-FAP was analyzed by calculating the conduction time between the SAN-FAP origin and the neighboring electrodes in the same plane. Because there are multiple electrodes with the same distance to the SAN-FAP origin in the different directions, the shortest conduction time from the origin of SAN-FAP toward the predefined distances within this area was calculated, reflecting the fastest conduction of the SR wave front away from the SAN-FAP origin.

ENDO-EPICARDIAL DELAY AT THE SINOATRIAL NODE AREA. Endo-epicardial delay (EED) was calculated by determining differences in local endo-epicardial activation times, as illustrated in Figures 1B and 1C. In accordance with previous mapping studies, for each electrode, the median of the time delays within the exact opposite electrode and its 8 surrounding electrodes was selected (8). For each set of electrodes at the same distance in each direction from the SAN-FAP origin, the median EED was selected. In line with previous studies, EEA was defined as EED ≥15 ms (9). Percentage of EEA was calculated within a radius of 10 mm from the SAN-FAP origin.

R/S RATIO. R/S ratios of unipolar potentials were calculated for all electrodes at the origin of the SAN-FAP. First, correction for the baseline amplitude was calculated per deflection between 70 and 30 ms before the deflection. Subsequently, the amplitudes of the R- and S-peak were extracted, and the baseline correction was applied. The R/S ratio was calculated by dividing the corrected amplitude of the R-peak by the corrected amplitude of the S-peak (12).

STATISTICAL ANALYSIS. Normally distributed continuous variables are expressed as mean ± SD and skewed variables as median (interquartile range). Continuous data were analyzed by using the Mann-Whitney *U* test or the Kruskal-Wallis H test. A p value < 0.05 was considered statistically significant. Statistical testing was performed by using IBM SPSS Statistics version 25 (IBM SPSS Statistics, IBM Corporation, Armonk, New York), and plots were created by using R version 3.6.1 (R Foundation for Statistical Computing, Vienna, Austria).

RESULTS

STUDY POPULATION. A total of 20 patients were included (15 [75%] male; median age 66 years [range: 59 to 73 years]; median body mass index 27 kg/m^2 [range: 23 to 31 kg/m^2]); 8 patients (40%) had a history of paroxysmal atrial fibrillation (AF) (Table 1). Ischemic heart disease, valvular heart disease, or combined heart diseases were present in 9 (45%), 4 (20%), and 7 (35%) patients, respectively. Most

patients had a good left ventricular function (LVF) or mild impairment (left ventricular ejection fraction 50% to 70% and 40% to 49%, respectively); only 3 patients showed moderate impairment of LVF (left ventricular ejection fraction 30% to 39%). None of the patients had heart failure or sinus node dysfunction.

CHARACTERISTICS OF SAN ACTIVATION. In 15 patients, repetitive SAN activity at the same exit site was observed, and 5 patients exhibited >1 different exit site (2 patients exhibited 2 different exit sites; 3 patients exhibited 3 different exit sites). Characteristics of all 28 included SAN-FAPs are specified in Table 2. As shown in Figure 2, 3 distinct activation patterns were observed after analyses of 28 SAN-FAPs, including SAN activation patterns with the following: 1) solely an endocardial exit site (upper panel, n = 10 [36%]); 2) solely an epicardial exit site (middle panel, n = 13 [46%]); and 3) simultaneously activated endo-epicardial exit sites (lower panel, n = 5 [18%]). Although SAN activity was expected to be repetitive, 3 SAN-FAPs (11%) had nonrepetitive activation patterns, suggesting beat-to-beat variations in the origin of the SAN-FAP.

The left panel of Figure 3 shows the distribution of SAN-FAP exit pathways in the RA for both layers separately. As expected, SAN-FAPs were solely observed in the superior (n = 22 [79%]) and mid (n = 6 [21%]) RA but not in the inferior RA. All 3 patients with moderate LVF impairment exhibited exit pathways in the superior RA. No significant difference in cycle length was observed between the superior and mid RA (superior: 828 ms [705 to 938 ms] vs. mid: 545 ms [417 to 1,009 ms]; p = 0.194). As shown in the middle panel of Figure 3, the morphology of unipolar potentials recorded from the SAN-FAP origins in the superior RA differed significantly from the electrogram morphology observed at the mid RA (superior RA S-wave morphology: R/S ratio 0.045 [0.026 to 0.062]; mid RA S-wave morphology: R/S ratio 0.15 [0.067 to 0.34]; p = 0.004).

Characteristics of all SAN-FAPs are depicted in the right panel of Figure 3; there were no significant differences in CV and degree of EED between the superior and mid RA SAN-FAPs. Interestingly, all 6 SAN-FAPs on the mid RA occurred in patients with a history of AF.

The upper panel of Figure 4 shows the relation between conduction times at every pre-defined distance from the SAN-FAP origin. The conduction times increased linearly from 1 to 8 ms (4 to 12 ms) over a distance of 10 mm, which corresponds with a CV of 125 cm/s (80 to 250 cm/s). The lower panel of Figure 4 shows the degree of EED at every predefined distance within 10 mm from the SAN-FAP origin. The highest degree of EED (10 ms [6 to 14 ms]) was found at the SAN-FAP origin and decreased with increasing distance from the SAN-FAP. The percentage of EEA within this area ranged from 2% to 18% (median 5%).

FIGURE 4 Conduction Characteristics Surrounding the Sinoatrial Node Area

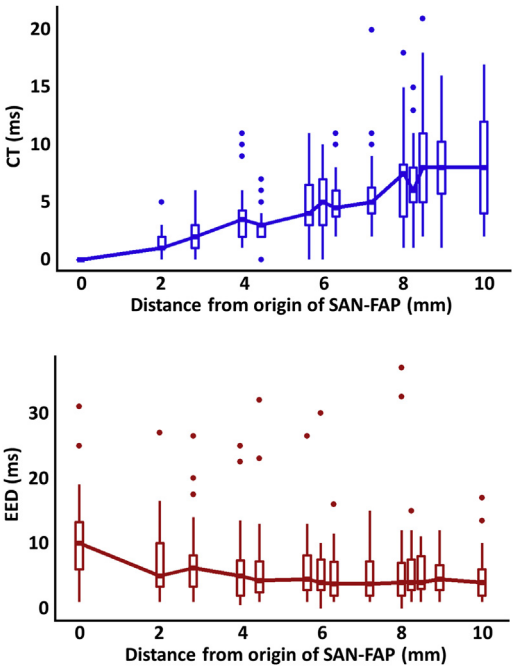

Conduction times **(upper panel)** and EED **(lower panel)** of SAN-FAPs for each measured electrode distance up to 10 mm. Median conduction velocity was 125 cm/s [interquartile range: 80 to 250 cm/s]. Highest EED was found at the SAN-FAP origin.
CT = conduction time; other abbreviations as in Figures 1 and 2.

Within a radius of 6 mm from the origin, 16 SAN-FAPs (57%) exhibited lines of CB in the same endo- or epicardial plane as the SAN-FAP, of whom 10 (63%) also showed CB lines in the opposite plane. Within a range of 10 mm from the origin of a SAN-FAP, lines of CB were found in 22 (79%) activation maps, either on both the endocardial and epicardial layer (n = 17 [77%]), solely on the same side of the SAN-FAP (n = 4 [18%]), and only once on the opposite side of the SAN-FAP (5%).

Figure 5 illustrates an SAN-FAP with a typical area of CB in both layers distal to its origin, which corresponds to the area lateral to the SAN. The area behind the line of CB is activated by a wave front ~78 ms later than start of SAN activation. These typical areas of CB present in both the endocardium and

FIGURE 5 Typical Areas of Conduction Block Surrounding the Sinoatrial Node Area

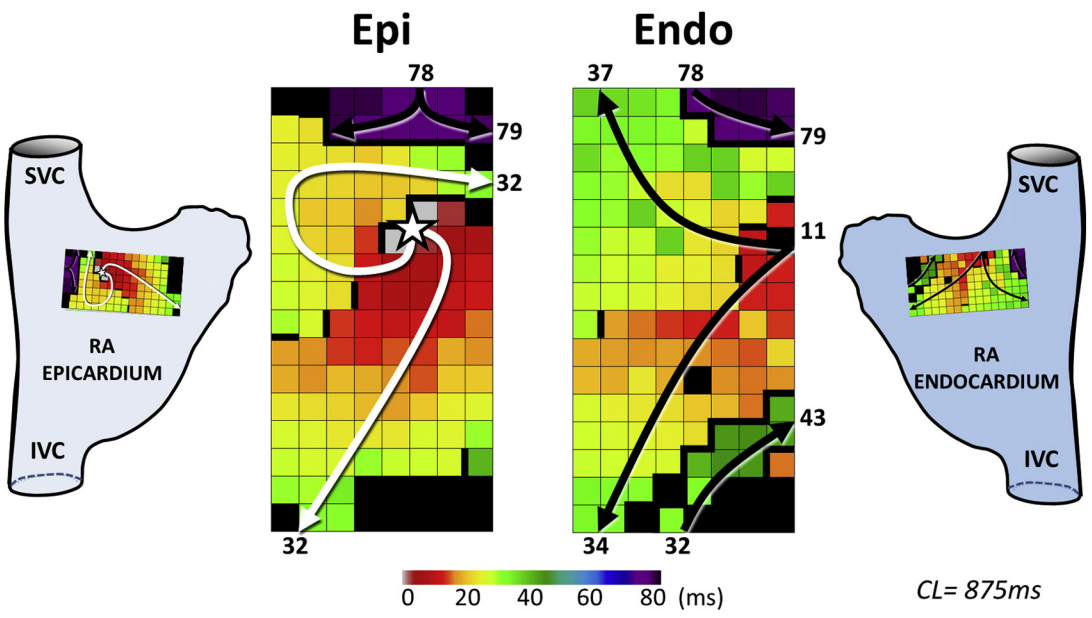

Example of endocardial and epicardial color-coded activation maps of the superior RA. The **arrows** display the main trajectories of the electrical wave fronts and local activation times are depicted at the head and tail. The **star** indicates the origin of SAN activation which is observed in the epicardial layer. **Thick black lines** indicate lines of conduction block (CB). The distal part of both activation maps show a typical area of CB in both atrial layers, which corresponds to the area lateral to the SAN. Abbreviations as in Figures 1 and 2.

epicardium were observed in 9 patients (45%). This area lateral to the SAN was activated with a delay ranging between 18 and 78 ms (median 34 ms [range: 29 to 53 ms]) after the onset of SAN activation.

DISCUSSION

KEY FINDINGS. Simultaneous endo-epicardial mapping of the SAN area revealed 3 different patterns of SAN activation: SAN activation with an epicardial exit site, an endocardial exit site, or simultaneous endo- and epicardial exit sites. SAN activity was mainly found in the epicardium of either the superior or mid RA, suggesting that SAN activation predominantly starts at the epicardium. However, in 36% of the SAN-FAPs, the earliest activated site was observed at the endocardium. Solely in patients with a history of AF, a caudal shift in SAN exit site was observed, which indicate changes in preferential sinoatrial exit pathways due to structural remodeling. Moreover, CB and EEA were commonly observed surrounding the SAN area (Central Illustration).

DYNAMIC RANGE OF SAN ACTIVATION. The SAN is a complex 3-dimensional structure located at the superior region of the sulcus terminalis isolated from the surrounding atria by blood vessels, fibrotic tissue, and fat (3,5). As expected, SAN activity was mainly observed in the superior RA (79%) and to a lesser degree in the mid RA (21%). Although the intrinsic length of the human SAN is only ~1 to 2 cm, the dynamic range of SAN activation may cover a larger area reaching up to the inferior cava vein (3,5,13–15). The large dynamic range of SAN activity was recently highlighted by ex vivo experiments in mice. Bychkov et al. (4) showed synchronized action potential emerging from heterogeneous subcellular subthreshold Ca^{2+} currents with a functional dynamic range extending from the superior to the inferior vena cava. In accordance, we also observed a large dynamic range of SAN activation reaching from the junction of the superior cava vein toward the mid RA, which is approximately 3 cm in length. Fedorov et al. (3) have also shown that sinoatrial exit pathways can be at distances of 2.61 ± 0.79 cm from each other, which is in line with our findings of the in vivo human heart.

CV AT THE RA FREE WALL AND NEAR THE ORIGIN OF SAN ACTIVITY. CV is dependent on fiber direction, enabling higher velocities in longitudinal rather than transverse cardiac muscle fiber direction. Right atrial CV has been measured at different anatomical

CENTRAL ILLUSTRATION **Endocardial-Epicardial Mapping of In Vivo Sinoatrial Node Activity**

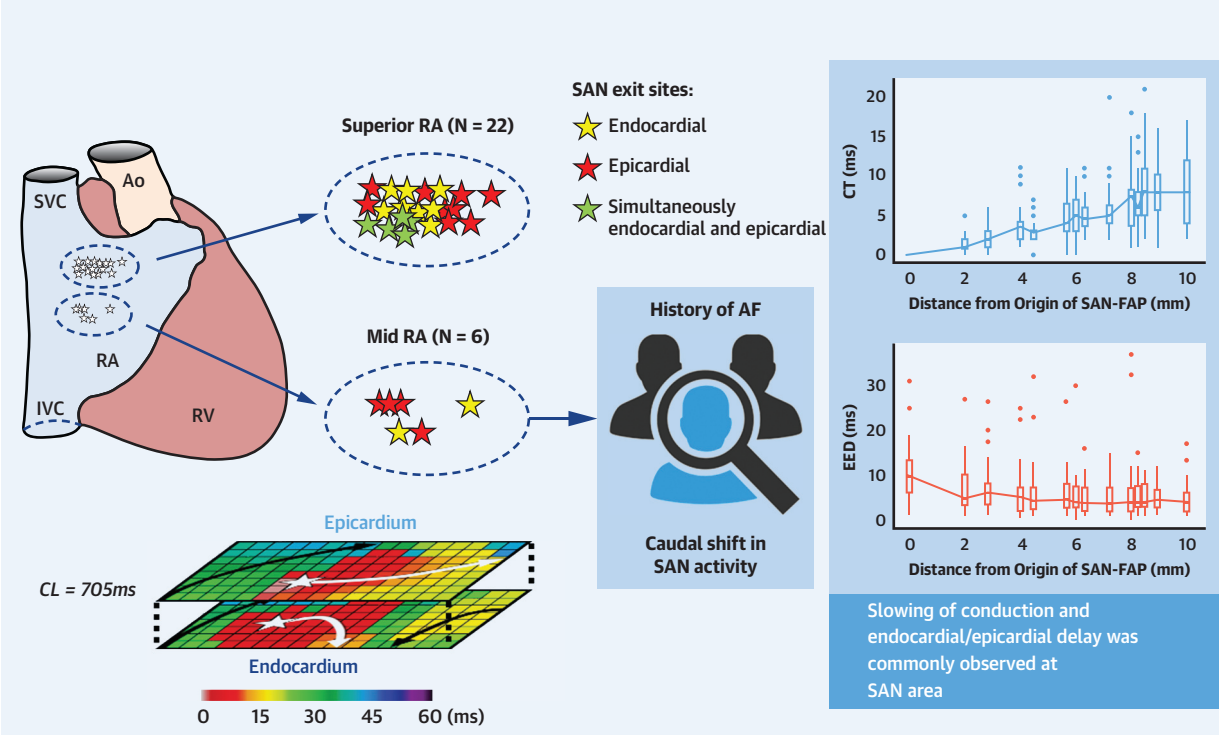

Kharbanda, R.K. et al. J Am Coll Cardiol EP. 2021;7(6):693–702.

AF = atrial fibrillation; Ao = aorta; CT = conduction time; EED = endocardial-epicardial delay; IVC = inferior cava vein; RA = right atrium; RV = right ventricle; SAN = sinoatrial node; SVC = superior cava vein.

locations and heterogeneity, and variety of the right atrial architecture should therefore be taken into account when comparing study outcomes. Konings et al. (16) reported an average epicardial CV of 72 ± 5 cm/s during SR at the right atrial free wall in patients with Wolff-Parkinson-White syndrome (244 unipolar electrodes, interelectrode distance 2.25 mm). Hansson et al. (17) found slightly higher epicardial CV in 12 patients undergoing open heart surgery due to ischemic heart disease (n = 8) or Wolf-Parkinson-White syndrome (n = 3). Before commencement of extracorporeal circulation, a mean CV of 88 ± 9 cm/s [(68 to 103 cm/s)], was observed during SR at the right atrial free wall (3 × 4 cm mapping array, 56 bipolar electrodes). We calculated local CV at the SAN area (<10 mm of SAN exit site) and observed a median atrial CV of 125 cm/s. This higher CV near the surrounding area of the SAN compared with CV measured at the RA free wall may be explained by longitudinal alignment of muscle fibers in the terminal crest that favors preferential conduction.

SAN: ANATOMICAL SUBSTRATE FOR ARRHYTHMOGENESIS?

Fedorov et al. (18) examined 3-dimensional arrhythmogenic features of the SAN during optical mapping of coronary perfused canine hearts. They showed that the SAN created a substrate for an atrial flutter (AFL) re-entry circuit, which anchored around the SAN structure. Moreover, the SAN exit pathways conducted bi-directionally, allowing SAN overdrive suppression during atrial pacing, AFL, and AF. However, they also showed that SAN exit pathways can block entering of wave fronts, thereby preventing electrically induced remodeling of the SAN. After administration of acetylcholine, hence increasing SAN entrance block, SAN activity was observed independently from the macro-re-entry circuit of AFL in the RA. Based on the presence of bi-directional slow-conducting SAN exit pathways, the authors postulated that this area may furnish an anatomical pathway for re-entrant arrhythmias.

The current study measured EED at the exit site of SAN activity and the surrounding atrial tissue within

a radius of 10 mm. The percentage of EEA (EED ≥15 ms) observed at the surrounding of the SAN area ranged from 2% to 18% (median 5%). Previous research has shown that EEA in the atrial wall plays an important role in the development of atrial tachyarrhythmias and may initiate re-entry (9,19,20). A recent study by Parameswaran et al. (6) also identified EEA at SAN exit sites (4 × 4 electrodes, 3-mm interelectrode distance). EEA was determined by: 1) comparing regional differences in distribution of SAN exit sites; 2) assessing the endo-epicardial wave front propagation sequence; and 3) determining the difference in phase value ≥20 ms between opposing endo-epicardial electrodes. Interestingly, after post-overdrive suppression at 600 and 400 ms, the amount of EEA in percentage increased, but paradoxically the degree of EED decreased. This raises the question of whether overdrive suppression of the SAN results in an increased degree of EEA, or solely an increased amount of EEA. Our study shows that not only slowing of atrial conduction but also EEA is present at and surrounding the SAN, which may contribute to atrial arrhythmogenesis.

SAN EXIT PATHWAYS IN PATIENTS WITH A HISTORY OF AF. Several studies have shown a caudal shift of SAN activity in patients with heart failure and sinus node dysfunction. Sanders et al. (21–23) performed endocardial mapping of SAN activation in 18 patients with symptomatic heart failure, 16 patients with sinus node dysfunction, and age-matched control subjects. Patients with heart failure or sinus node dysfunction, both conditions that are associated with development of AF, exhibited more caudal SAN exit sites. A caudal shift of SAN activity has also been observed after SAN overdrive pacing and episodes of AFL (3,15). Interestingly, we also observed a caudal shift in SAN activity in patients with a history of AF. None of the patients included in the current study had heart failure or were diagnosed with sinus node dysfunction or AFL. The underlying mechanism of caudal shifting of SAN activity in patients with heart failure or persistent arrhythmias remains poorly understood (15,21).

Stiles et al. (15) hypothesized that the superior relatively shorter SAN exit pathway is more susceptible to undergo structural remodeling, resulting in conduction abnormalities. It is most likely that atrial structural remodeling in patients with a history of AF may result in conduction block in superior SAN exit pathways that may ensue a caudal shift of SAN exit sites, as observed in the current study.

STUDY LIMITATIONS. Although strict selection criteria were used to select SAN-FAPs, due to lack of histology, it still might be possible that some SAN-FAPs were not caused by SAN activity but by ectopic focal discharges in the right atrial wall. Furthermore, due to the limited size of the electrode arrays, it may be possible that the actual earliest activation site was outside the measurement area. However, because during stable SR, all SAN-FAPs were found in the superior and mid RA and mostly repetitive, this is very unlikely. An inevitable effect of in vivo mapping is lack of histology and intramural SAN analyses. In addition, we could not perform simultaneous endo-epicardial mapping of the entire RA simultaneously to investigate the effect of beat-to-beat variation on SAN exit sites. Another limitation of our study is that we measured fastest apparent CV in the 2-dimensional plane, whereas SAN activation occurs in the 3-dimensional plane. Therefore, our method overestimates real CV surrounding the SAN. Lastly, this study described conduction in the SAN region. Recordings with an even higher spatial resolution are required to analyze wave propagation within the SAN itself.

CONCLUSIONS

The current study is one of the first to analyze in vivo patterns of activation surrounding the SAN from an endo- and epicardial perspective by performing simultaneous endo-epicardial mapping of the human RA in patients undergoing cardiac surgery. The observed variations in patterns of activation highlight the complex 3-dimensional spread of SR wave fronts emerging from the SAN and the presence of interindividual differences in SAN exit pathways. Solely in patients with a history of AF, SAN activity occurred more caudally, which may reflect changes in preferential sinoatrial exit pathways as a result of structural remodeling.

FUNDING SUPPORT AND AUTHOR DISCLOSURES

The authors have reported that they have no relationships relevant to the contents of this paper to disclose.

ADDRESS FOR CORRESPONDENCE: Dr. Natasja M.S. de Groot, Unit Translational Electrophysiology, Department of Cardiology, Erasmus Medical Center, Doctor Molewaterplein 40, 3015 GD Rotterdam, the Netherlands. E-mail: n.m.s.degroot@erasmusmc.nl.

PERSPECTIVES

COMPETENCY IN MEDICAL KNOWLEDGE: In line with previous ex vivo SAN mapping studies, the current study shows the presence of intraindividual and interindividual differences in SAN exit pathways in patients undergoing cardiac surgery. In addition to slowing of atrial conduction, EEA is present surrounding the SAN, which may contribute to atrial arrhythmogenesis. Activation of inferior SAN exit pathways was only observed in patients with a history of AF, which may be a result of structural remodeling within superior SAN exit pathways.

TRANSLATIONAL OUTLOOK: Future in vivo simultaneous endo-epicardial mapping studies are essential to investigate SAN activation and unravel its role in atrial arrhythmogenesis. Further studies are required to investigate the effect of underlying heart disease (e.g., ischemic, valvular, or congenital heart disease) on SAN activation and SAN dysfunction.

REFERENCES

1. Boineau JP, Canavan TE, Schuessler RB, Cain ME, Corr PB, Cox JL. Demonstration of a widely distributed atrial pacemaker complex in the human heart. Circulation 1988;77:1221–37.

2. Schuessler RB. Abnormal sinus node function in clinical arrhythmias. J Cardiovasc Electrophysiol 2003;14:215–7.

3. Fedorov VV, Glukhov AV, Chang R, et al. Optical mapping of the isolated coronary-perfused human sinus node. J Am Coll Cardiol 2010;56:1386–94.

4. Bychkov R, Juhaszova M, Tsutsui K, et al. Synchronized cardiac impulses emerge from heterogeneous local calcium signals within and among cells of pacemaker tissue. J Am Coll Cardiol EP 2020;6:907.

5. Sánchez-Quintana D, Cabrera JA, Farré J, Climent V, Anderson RH, Ho SY. Sinus node revisited in the era of electroanatomical mapping and catheter ablation. Heart 2005;91:189–94.

6. Parameswaran R, Lee G, Morris GM, et al. Simultaneous epicardial-endocardial mapping of the sinus node in humans with structural heart disease: impact of overdrive suppression on sinoatrial exits. Heart Rhythm 2020;17:2154–63.

7. Knops P, Kik C, Bogers AJ, de Groot NM. Simultaneous endocardial and epicardial high-resolution mapping of the human right atrial wall. J Thorac Cardiovasc Surg 2016;152:929–31.

8. Kharbanda RK, Knops P, van der Does LJME, et al. Simultaneous endo-epicardial mapping of the human right atrium: unravelling atrial excitation. J Am Heart Assoc 2020;9:e017069.

9. de Groot N, van der Does L, Yaksh A, et al. Direct proof of endo-epicardial asynchrony of the atrial wall during atrial fibrillation in humans. Circ Arrhythm Electrophysiol 2016;9:e003648.

10. Allessie MA, de Groot NM, Houben RP, et al. Electropathological substrate of long-standing persistent atrial fibrillation in patients with structural heart disease: longitudinal dissociation. Circ Arrhythm Electrophysiol 2010;3:606–15.

11. Mouws EMJP, Lanters EAH, Teuwen CP, et al. Epicardial breakthrough waves during sinus rhythm: depiction of the arrhythmogenic substrate? Circ Arrhythm Electrophysiol 2017;10:e005145.

12. van Schie MS, Starreveld R, Roos-Serote MC, et al. Classification of sinus rhythm single potential morphology in patients with mitral valve disease. Europace 2020;22:1509–19.

13. Boineau JP, Schuessler RB, Hackel DB, Miller CB, Brockus CW, Wylds AC. Widespread distribution and rate differentiation of the atrial pacemaker complex. Am J Physiol 1980;239:H406–15.

14. Cosío FG, Martín-Peñato A, Pastor A, et al. Atrial activation mapping in sinus rhythm in the clinical electrophysiology laboratory. J Cardiovasc Electrophysiol 2004;15:524–31.

15. Stiles MK, Brooks AG, Roberts-Thomson KC, et al. High-density mapping of the sinus node in humans: role of preferential pathways and the effect of remodeling. J Cardiovasc Electrophysiol 2010;21:532–9.

16. Konings KT, Kirchhof CJ, Smeets JR, Wellens HJ, Penn OC, Allessie MA. High-density mapping of electrically induced atrial fibrillation in humans. Circulation 1994;89:1665–80.

17. Hansson A, Holm M, Blomstrom P, et al. Right atrial free wall conduction velocity and degree of anisotropy in patients with stable sinus rhythm studied during open heart surgery. Eur Heart J 1998;19:293–300.

18. Fedorov VV, Chang R, Glukhov AV, et al. Complex interactions between the sinoatrial node and atrium during reentrant arrhythmias in the canine heart. Circulation 2010;122:782–9.

19. Schuessler RB, Kawamoto T, Hand DE, et al. Simultaneous epicardial and endocardial activation sequence mapping in the isolated canine right atrium. Circulation 1993;88:250–63.

20. Hansen BJ, Zhao J, Csepe TA, et al. Atrial fibrillation driven by micro-anatomic intramural re-entry revealed by simultaneous sub-epicardial and sub-endocardial optical mapping in explanted human hearts. Eur Heart J 2015;36:2390–401.

21. Sanders P, Kistler PM, Morton JB, Spence SJ, Kalman JM. Remodeling of sinus node function in patients with congestive heart failure. Circulation 2004;110:897–903.

22. Sanders P, Morton Joseph B, Kistler Peter M, et al. Electrophysiological and electroanatomic characterization of the atria in sinus node disease. Circulation 2004;109:1514–22.

23. John RM, Kumar S. Sinus node and atrial arrhythmias. Circulation 2016;133:1892–900.

KEY WORDS endo-epicardial mapping, endo-epicardial asynchrony, sinoatrial node